Shi, Z., Chen, J., You, R., Chen, C., and Chen, Q. 2016. "Modeling of gasper-induced jet flow and its impact on cabin air quality," *Energy and Buildings*, 127: 700-713.

Modeling of Gasper-Induced Jet Flow and Its Impact on Cabin Air Quality

Zhu Shi[1], Jun Chen[1], Ruoyu You[1], Chun Chen[2] and Qingyan Chen[1,3]

[1] School of Mechanical Engineering, Purdue University, West Lafayette, IN 47907, USA

[2] Department of Mechanical and Automation Engineering, The Chinese University of Hong Kong, Shatin, N.T. 999077, Hong Kong SAR, China

[3] Tianjin Key Laboratory of Indoor Air Environmental Quality Control, School of Environmental Science and Engineering, Tianjin University, Tianjin 300072, China

Abstract

Gaspers are prevalently installed in aircraft and automobiles to provide supplementary ventilation and improve passengers' thermal comfort. This investigation employed the SST $k-\omega$ model to simulate gasper-induced jet flow with the use of detailed gasper geometry, and validated the simulation results using experimental data. The validated CFD results not only revealed the mixing mechanism of a gasper-induced jet with ambient air, but also enabled the development of two mathematical models for characterizing the jet development along the gasper axis and radial velocity profiles in the downstream region. Furthermore, these models enabled the prediction of the entrainment ratio at different locations along a gasper-induced jet, and this ratio was used to evaluate the impact of the jet on air quality in a passenger's breathing zone. The performance of the CFD model and mathematical models was evaluated, and the models were compared on the basis of prediction accuracy and computing time.

Keywords: Gasper, jet flow, computational fluid dynamics, mathematical modeling, entrainment

Nomenclature

A	Gasper opening area
D	Characteristic diameter of gasper outlet
D_e	Equivalent diameter
G_k	Generation of turbulent kinetic energy due to mean velocity gradient
G_ω	Generation of ω

K_1, K_2	Coefficients
k	Specific kinetic energy
M	Momentum flux
p	Pressure
P_{st}	Static pressure
$\dot{Q}$	Air flow rate
Re	Reynolds number
S_ϕ	Source term of scalar ϕ
U_c	Centerline velocity
$U_{\max}$	Maximum velocity on centerline
U_0	Initial velocity at gasper outlet
u_i	Velocity magnitude in direction i
u_z'	turbulent fluctuation in z direction
x_i	Coordinate in the i direction
$x_{0.1}$, $x_{0.5}$, and $x_{0.9}$	Radial locations where z-velocities are 0.1, 0.5, and 0.9 respectively, of local maximum
$x'_{0.1}$, $x'_{0.5}$, and $x'_{0.9}$	Radial locations where turbulence intensities are 0.1, 0.5, and 0.9, respectively, of local maximum
Y_k, Y_ω	Dissipations of k and ω due to turbulence
z_{peak}	Coordinate in the z direction of peak velocity
$\overline{z}$	Normalized z-direction location
$\Gamma_{\phi,eff}$	Coefficient of effective diffusion of scalar ϕ
ε	Entrainment ratio
δ	Gasper opening size
η	Gasper-induced jet airflow rate ratio
λ	Mixing layer thickness
μ	Dynamic viscosity
μ_t	Turbulent dynamic viscosity
ν	Kinematic viscosity
ν_t	Turbulent kinematic viscosity
ρ	Density
σ_k	Turbulent Prandtl number for k
σ_C	Schmidt number
$\sigma_{C,t}$	Turbulent Schmidt number
χ	Normalized x-direction location
ω	Specific dissipation rate
$\langle\phi\rangle$	Time averaged value of ϕ

1 Introduction

Traveling by air has become increasingly popular among passengers around the world. It was reported that the number of passengers carried by air transport reached 2.98 billion in 2012 (IATA 2013). The International Civil Aviation Organization has estimated that this number will reach 6 billion by 2030 (ICAO 2012). As air travel becomes more frequent, the issue of airborne infectious disease transmission in aircraft cabins has been addressed collectively by researchers from various disciplines. In particular, the spread of severe acute respiratory syndrome (SARS) (Olsen et al. 2003) and H1N1 influenza (Baker et al. 2010) in airplane cabins has suggested that the transmission of airborne infectious diseases could be associated with the airflow patterns in these spaces (Li et al. 2007). Therefore, it is necessary to investigate the airflow distribution in aircraft cabins in order to improve the design of cabin ventilation systems and reduce the risk of infection.

Current aircraft cabins use mixing ventilation, which supplies fresh air from diffusers at or near ceiling level and returns air through exhaust openings at the floor level on the cabin walls. Such a ventilation system creates large re-circulation patterns in the cabins, so that the air temperature and contaminant concentration distributions are uniform However, it was found that mixing ventilation could easily lead to the transmission of airborne infectious diseases among passengers (Zhang and Chen 2007). In addition to mixing ventilation, researchers have investigated the airflow distribution in an aircraft cabin with other ventilation modes. For example, Gao and Niu (2008) studied the distribution of air from a personalized ventilation nozzle and concluded that the personalized system could reduce a passenger's exposure to air pollutants by up to 60%. Zhang and Chen (2007) also found that personalized ventilation could provide better cabin air quality than mixing or displacement ventilation without the risk of draft. Other studies (Melikov et al. 2012; Zitek et al. 2010) also reported an increased comfort level when personalized air supplies were incorporated in the seat headrest and seat back. Hence, personalized ventilation has the potential to reduce the risk of airborne infectious disease transmission in aircraft cabins, while at the same time improving passengers' thermal comfort.

Gaspers are the most commonly used personalized ventilation devices in aircraft cabins, and they are installed at ceiling level and directly above passengers' seats. By adjusting the opening area and angle of a gasper, a passenger can change the airflow rate and direction of the jet induced by the gasper. A typical gasper consists of an adjustable annular air outlet and an internal cone, which makes gasper-induced jet flow much more complicated than the jet from a simple round hole. It is important to understand how the jet develops after the air is discharged from a gasper outlet because the jet will interact with the main flow in the cabin.

To investigate gasper-induced jet flow, both experimental and numerical methods have been used. On the experimental side, for example, Anderson (2012) used carbon dioxide (CO_2) as a tracer gas to study the effect of a personal gasper on airborne contaminant transport in an aircraft cabin. They found that the gasper played an important role in overall contaminant transmission.

Guo et al. (2014) used an anemometer to obtain high-resolution measurements of turbulence parameters in a jet airflow field induced by a gasper. These measurements provided reliable airflow data, but the method was time-consuming. On the other hand, computational fluid dynamics (CFD) has made it possible to predict the airflow distribution of gasper-induced jet flow. For instance, Baker et al. (2006) and Gupta et al. (2011) used a circular outlet to model gasper outlet flow in an aircraft cabin. By simplifying the gasper geometry as a round nozzle, they significantly reduced computational effort required for their simulations. However, such a simplification may cause errors, since the features of round jets are different from those of annular jets, particularly in jet developing region (Warda et al. 1999). Moore et al. (2004) and García-Villalba et al. (2006) have used annular nozzles, but the geometry of the nozzles was not the same as the gasper geometry in aircraft cabins. You et al. (2016) used detailed gasper geometry in simulating airflow in a mockup of a partial aircraft cabin with gasper on, but their study was more focused on the major flow in cabin. Therefore, it is needed to develop a CFD model that incorporates realistic gasper geometry, to study the flow characteristics of gasper-induced jets, especially in the initial development region of the jet flow.

Furthermore, both the air velocity and opening size of a gasper can vary. The jet velocity can be controlled by the environmental control system (ECS) (Wang et al. 2008; Wu and Ahmed 2011), and the opening size is controlled by the passenger. Understanding how gasper-induced jet flow develops under various air velocities and opening sizes is essential for better characterization of the gasper-induced jet flow field and optimization of gasper geometry.

The present study built a CFD model for studying the jet flow from a gasper with detailed gasper geometry. The CFD simulation results were first compared with experimental results for the purpose of model validation. The CFD model was then used to explore how the second-order flow feature in the gasper-induced jet was influenced by initial air velocity and gasper opening size. Two mathematical models, based on jet initial velocity and gasper opening size, were developed, so that the airflow pattern and air quality in a gasper-induced jet could be effectively studied and efficiently predicted. The performance of the CFD model and mathematical models was evaluated in terms of prediction accuracy and calculation time, and on the basis of the evaluation, this study has provided suggestions for model selection.

2 Research Method

As indicated by the review in the previous section, a CFD model can be an effective tool for studying the jet flow from a gasper with complex geometry. However, the CFD model should be validated by experimental data, as such a model normally uses a large number of approximations and assumptions.

2.1 Experimental setup

To validate the CFD model, this investigation used experimental data from Dai et al.(2015). Figure 1 shows the experimental rig that was used. It consisted of a gasper, a plenum chamber made of Plexiglas, and an air supply pipe. An air compressor and an air storage tank were used to provide a clean, dry, and stable airflow to the gasper nozzle. Hot-wire anemometers were used to measure the air velocity in the downstream region. By employing an electronically controlled 3D translation stage, the measurements yielded data with a spatial resolution of 0.01 mm. The measurements were taken in a calm, isothermal environment.

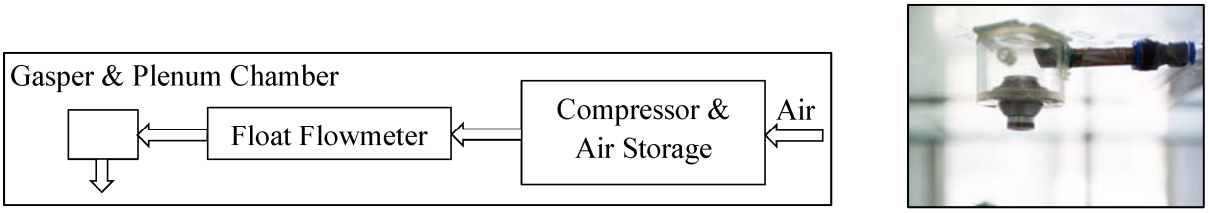

(a) (b)

Fig. 1 Experimental setup for measuring the gasper-induced jet (Dai et al. 2015): (a) schematic of the setup and (b) photo of the gasper and plenum chamber

2.2 Numerical method

To calculate the gasper-induced jet flow, this study used the shear stress transport (SST) $k-\omega$ model (Wilcox 1998; Menter 1994), because it has the best performance among the commonly used turbulence models in modeling a stratified jet (Shi et al. 2015). According to Patankar (1980) and White (1991), the transport equations for momentum, k, and ω can be expressed in a general form:

$$\rho\frac{\partial\langle\phi\rangle}{\partial t}+\rho\overline{u}_i\frac{\partial\langle\phi\rangle}{\partial x_i}-\frac{\partial}{\partial x_i}\left[\Gamma_{\phi,eff}\frac{\partial\langle\phi\rangle}{\partial x_i}\right]=S_\phi \tag{1}$$

where the general variable ϕ, the source term S_ϕ, and the coefficient of effective diffusion $\Gamma_{\phi,eff}$ of the $k-\omega$ model are summarized in Table 1 (ANSYS 2011). No energy equation was solved because both the experiment and the CFD simulation were conducted under isothermal conditions.

Table 1. Definitions of ϕ, $\Gamma_{\phi,eff}$, and S_ϕ in Equation (1).

ϕ	$\Gamma_{\phi,eff}$	S_ϕ	Constants
u_j	$\mu+u_t$	$-\frac{\partial p}{\partial x_i}+\frac{\partial}{\partial x_j}\left[(\mu+\mu_t)\frac{\partial u_j}{\partial x_i}\right]$	-

k	$\mu+\mu_t/\sigma_k$	G_k-Y_k	$\mu_t=\frac{\rho k}{\omega}\frac{1}{\max\left[\frac{1}{\alpha^*},\frac{SF_2}{a_1\omega}\right]}$, $\sigma_k=\frac{1}{F_1/\sigma_{k,1}+(1-F_1)/\sigma_{k,2}}$, $\sigma_\omega=\frac{1}{F_1/\sigma_{\omega,1}+(1-F_1)/\sigma_{\omega,2}}$, $G_k=\mu_t S^2$, $G_\omega=\frac{\alpha}{\nu_t}\tilde{G}_k$, $\tilde{G}_k=\min(G_k,10\rho\beta^*k\omega)$, $Y_k=\rho\beta^*k\omega$, $Y_\omega=\rho\beta\omega^2$, $\sigma_{k,1}=1.176$, $\sigma_{\omega,1}=2.0$, $\sigma_{k,2}=1.0$, $\sigma_{\omega,2}=1.168$, $a_1=0.31$
ω	$\mu+\mu_t/\sigma_\omega$	$G_\omega-Y_\omega$	

The SIMPLE scheme was used for coupling the pressure and velocity equations. The second-order discretization method was used for the pressure, momentum, turbulent kinetic energy, and specific dissipation rate equations. This investigation assumed that the calculation was converged when the residuals of the continuity, u_x, u_y, u_z, k, and ω in Equation (1) decreased to 3.1×10^{-8}, 2.3×10^{-7}, 2.3×10^{-7}, 4.2×10^{-7}, 1.1×10^{-6}, and 1.6×10^{-5}, respectively. This investigation used the ANSYS Fluent program V14.0 (ANSYS Inc. 2011) to perform the numerical calculations.

To accurately model the gasper-induced airflow, it was necessary to implement the detailed geometry of the gasper in the CFD model. Figure 2(a) is a photograph of the actual gasper installed in the cockpit of an MD-82 commercial airliner. In the present study, we built a CAD model for the gasper with detailed geometry as shown in Figure 2(b). When the gasper was switched on, conditioned air was discharged through the annular opening (indicated in red in Fig. 2(b)). There was a solid cone inside the rotatable switch.

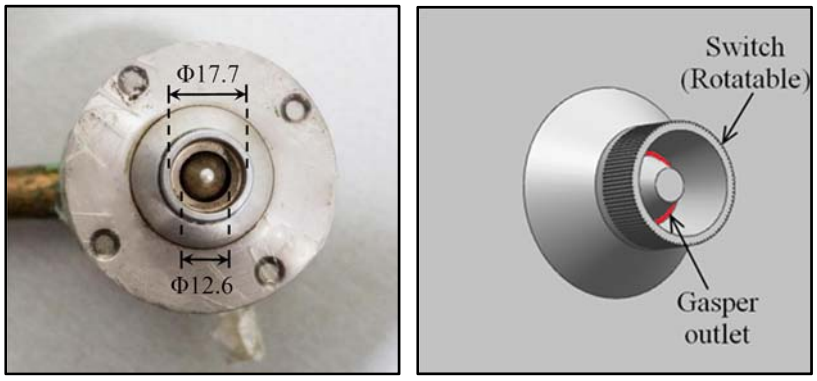

(a) (b)

Fig. 2 (a) Photograph of the actual gasper (unit: mm) (Dai et al. 2014) and (b) detailed geometry of the gasper model used in this study.

To model the case measured by Dai et al. (2015), this study placed the gasper model (nozzle diameter D=12.6 mm) into a cylindrical calculation domain with a diameter of 500 mm (40D)

and a length of 600 mm (48D), as shown in Figure 3. According to Fan et al. (2005), this dimension is large enough for simulating a free jet. Since the geometry in this case was symmetric, one quarter of the geometry was used to construct the computation domain, as shown in Figure 3(a). The plane z = 0 was defined on the edge of the gasper's rotatable switch (Figures 2b and 3a). The velocity inlet boundary was set at the gasper outlet (the red area in Fig. 2b). The side and bottom boundaries of the calculation domain were defined as the pressure outlet, and standard atmospheric pressure was prescribed. A symmetry (zero-shear, no normal velocities) boundary was used for the two symmetric faces. All other boundaries were defined as no-slip wall boundaries. Independence tests were conducted to determine the size of the calculation domain. It was found that enlarging the domain to a cylinder with a length of 900 mm and diameter of 750 mm did not lead to a noticeable difference in simulation results. Hence, this further verified that the originally proposed size of the calculation domain was sufficient to provide accurate results for the gasper-induced jet flow.

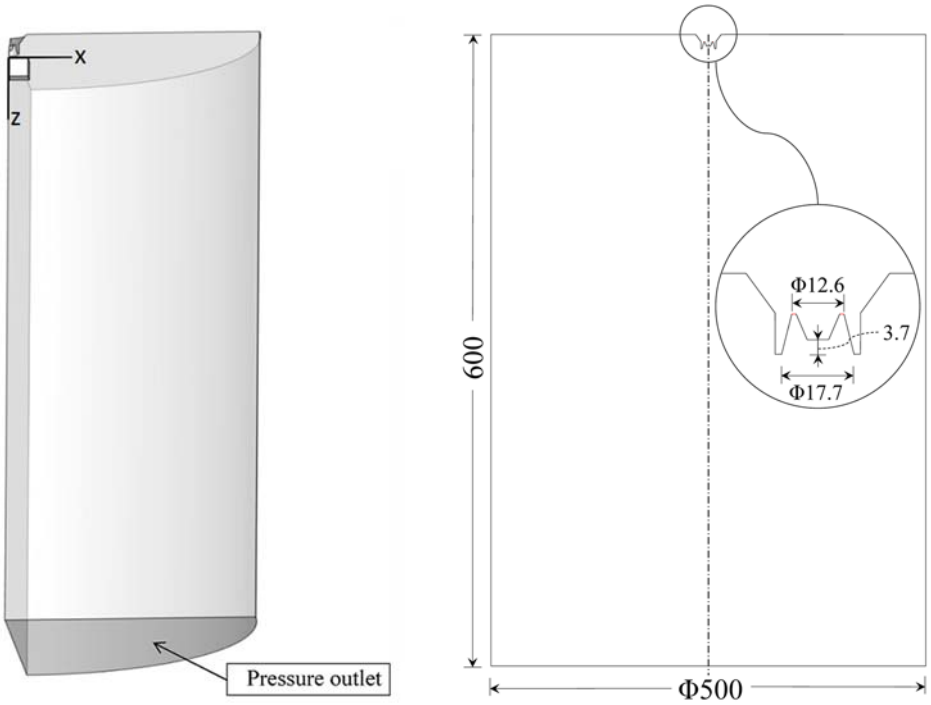

(a) (b)

Fig. 3 (a) Computation domain in the current study and (b) details of the simulated gasper (unit: mm).

Figure 4 shows the grid structure used in this study, where the grid sizes were non-uniform. The smallest meshes were used around the gasper nozzle (0.12 mm), and the mesh size gradually increased with distance from the gasper. A grid independence test was conducted by comparing

the velocity profile along the jet direction with three different grid numbers (444,565, 1,445,920, and 2,914,101). As shown in Figure 5, the resolution of 1,445,920 was sufficient for obtaining a grid-independent result for the velocity profile.

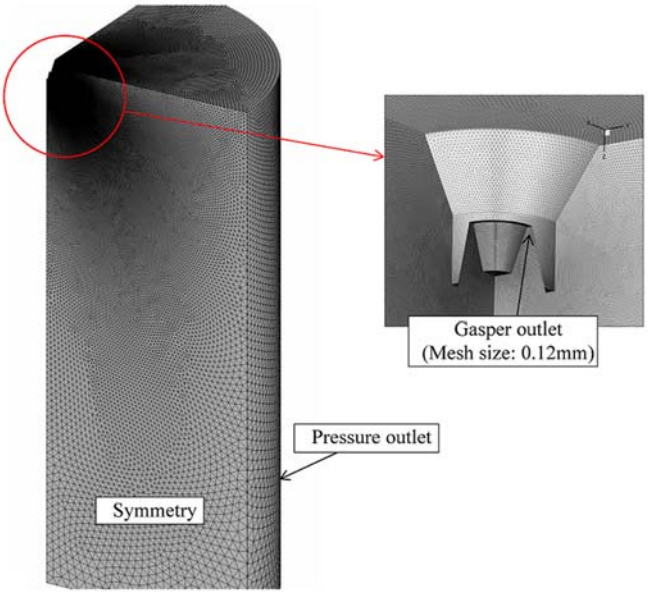

Fig. 4 Grid structure used in the study.

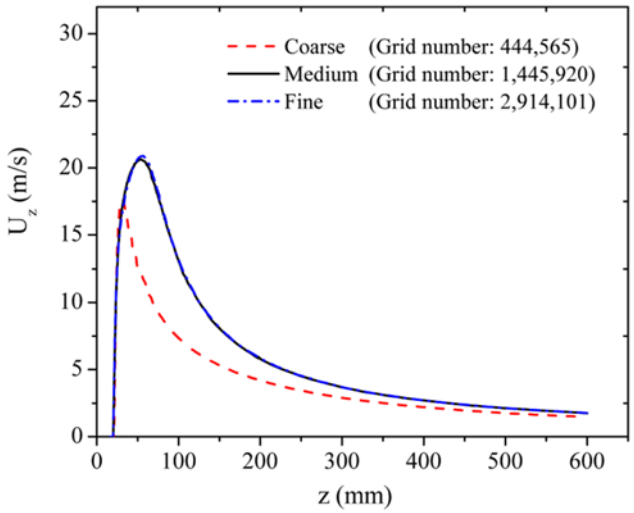

Fig. 5 Grid independence test results for the gasper-induced jet flow simulation.

3. Results

This section first discusses the accuracy of the CFD simulation by comparing the numerical results with the corresponding experimental data for the jet that developed from the gasper. We then describe the use of the validated CFD model to study the jet flow characteristics.

3.1 Validation with experimental data

Figure 6 shows the simulated velocity profile at different downstream locations. The velocity profile starts with double peaks, which were caused by the annular gasper outlet. The two peaks gradually merge to one peak. Figure 7(a) compares the calculated centerline velocity U_c along the jet axis (z direction) with the experimental data, where U_c has been normalized by its maximum value U_{max} and z by the location of U_{max} and D. Because of the Coanda effect (Wille and Fernholz 1965), the air from the annular inlet immediately attached to the solid cone. At a certain distance from the inlet, the airflow around the cone merged to a single stream. This explains why U_{max} did not occur at the inlet (z = 0). The comparison shows that the modeling results agreed well with the experimental data, especially after the merging point (z=3.2D) where the flow was more developed. The mixing mechanism of this flow is illustrated in detail in Section 3.2.

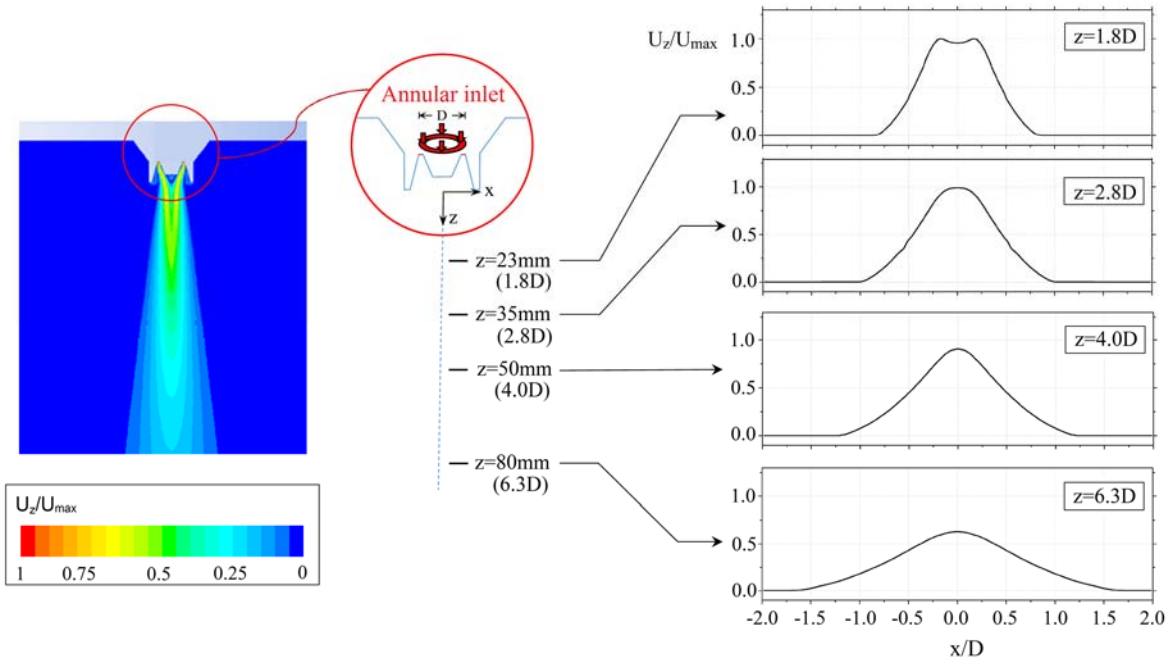

Fig. 6 Development of the velocity profile along the jet axis

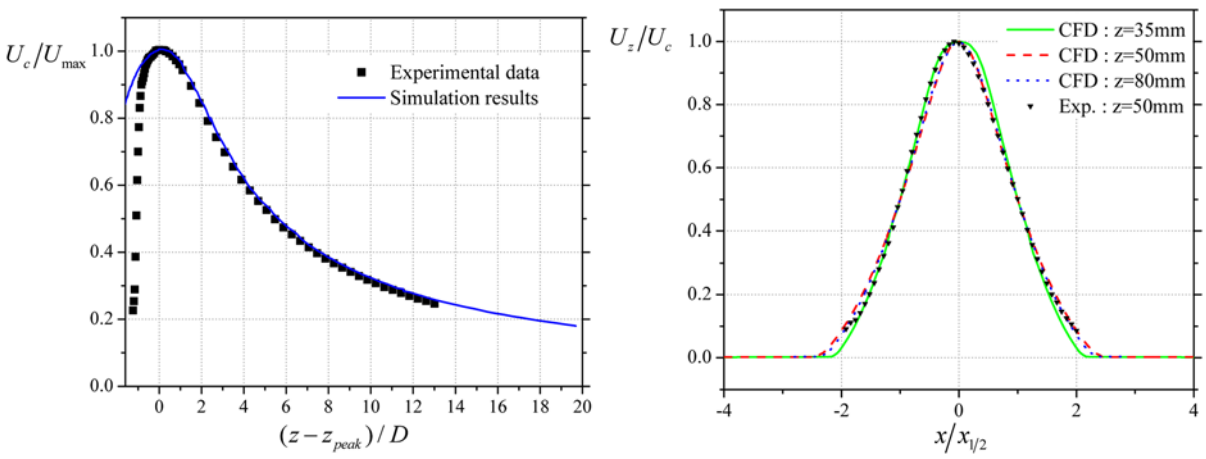

(a) (b)

Fig. 7 Comparison of the simulated velocity with the experimental data (Dai et al. 2014): (a) centerline velocity and (b) self-similarity velocity profiles in the downstream region of the jet.

This investigation also performed a self-similarity test on the peak velocity profiles in the region downstream from the jet. Pope (2000) has discussed self-similar characteristics in turbulent round jets in detail. Figure 7(b) shows $U_z/U_c - x/x_{1/2}$ profiles, where $x_{1/2}$ is the x location at which the z-velocity is half of U_c. After normalization, the three profiles at the three different downstream locations collapse into almost a single profile, which strongly indicates self-similarity. The similarity profiles also matched well with the experimental data. Since the numerical model used in this study is able to predict the gasper-induced airflow with reasonably good accuracy, the model is considered to be validated.

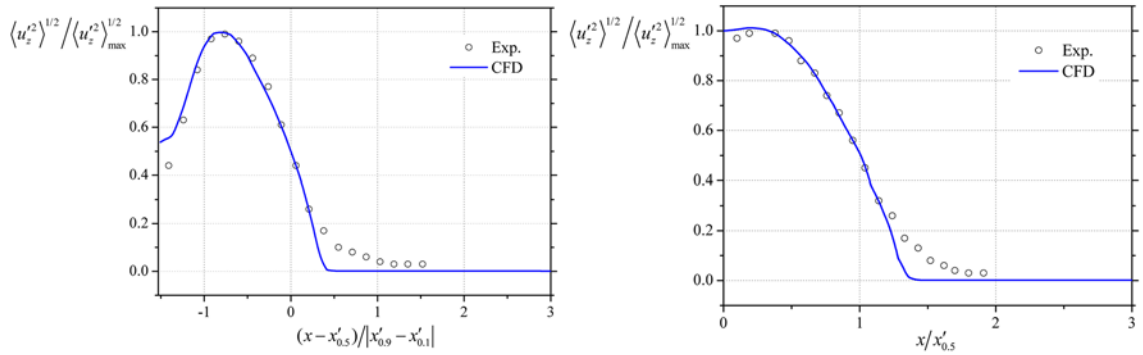

(a) (b)

Fig. 8 Comparison of turbulence intensity in: (a) developing region (z = 2D) and (b) fully developed region (z = 9D).

In addition to mean velocities, this study also investigated the second-order flow feature in the gasper-induced jet. Figure 8 is a plot of normalized turbulence intensity $\left\langle u_z'^2 \right\rangle^{1/2} \Big/ \left\langle u_z'^2 \right\rangle_{\max}^{1/2}$, where $\left\langle u_z'^2 \right\rangle^{1/2}$ represents turbulent fluctuation in the z direction and $\left\langle u_z'^2 \right\rangle_{\max}^{1/2}$ represents the maximum turbulence intensity at a particular location, against normalized radial distances in the developing region (before the merging point) and fully developed region (after the merging point). The non-dimensional radial distances used were $(x - x'_{0.5}) \big/ \left| x'_{0.9} - x'_{0.1} \right|$ and $x / x'_{0.5}$. In particular, $x'_{0.1}$, $x'_{0.5}$, and $x'_{0.9}$ were the radial locations where $\left\langle u_z'^2 \right\rangle^{1/2}$ reached 0.1, 0.5, and 0.9, respectively, of the corresponding local maximums. The comparison shows that in the developing region, where a bell-shaped jet dominated and had not merged towards the center, there was a "dent" at the flow center. In the fully developed region, the turbulence intensity profile was similar to that for a fully developed round jet (Shi et al. 2015): the "dent" still existed, but it became significantly shallower. Overall, the CFD prediction of turbulence intensity agreed well with the experimental data, which further validated the CFD model for simulating the gasper-induced jet flow on the second-order flow characteristics level. The discrepancies between the CFD results and experimental data can be attributed to the assumption in the SST $k-\omega$ model that kinetic eddy viscosity is isotropic (Hinze 1975), which is not strictly true.

3.2 Mixing mechanism of the gasper-induced jet

The validation of the CFD model enabled further study of the mixing mechanism in the gasper-induced jet through investigation of the streamlines of the mean flow field, mean velocity, and static pressure. Figure 9(a) illustrates the streamlines in the initial developing region of the jet. It can be seen that before the merging point, the flow was still developing and vortices were generated. These vortices indicate a complicated flow pattern. Thus, this region was more difficult to model accurately in Section 3.1. The formation of these vortices can be explained by static pressure distribution, as illustrated in Figure 9(b): before the peak pressure point, a positive axial pressure gradient maintained the reverse flow, which formed vortices, and the local minimum pressure location coincided with the centers of the vortices. In this investigation, the z-stagnation point was defined as the location at which $U_z = 0$. In particular, the two z-stagnation points on the jet centerline were defined as z_{s1} and z_{s2}. The distance between them, $z_{s2} - z_{s1}$, characterized the size of the vortices that were formed; in this case, the size was 0.3D. The second z-stagnation point marked the end of vortices, and also approximately coincided with the peak pressure point, which was in good agreement with what the observations of Rehab et al. (1997) and Chigier and Beer (1964). After the second z-stagnation point, the static pressure dropped so dramatically that ambient fluid was quickly entrained towards the jet center. This

explains the increase in centerline velocity after the second z-stagnation point in Figure 9(b), and the expansion of the z-stagnation lines in Figure 9(a).

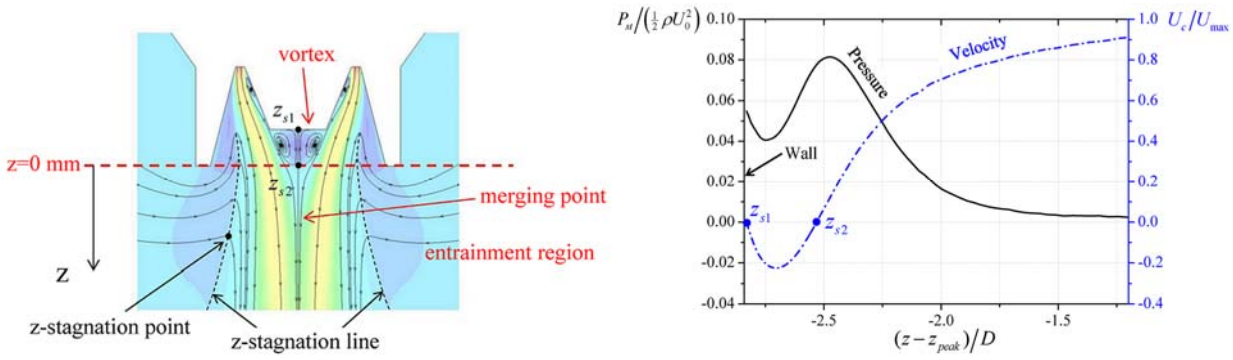

(a) (b)

Fig. 9 Flow characteristics near the gasper inlet: (a) air velocity streamlines and (b) pressure and velocity distributions.

To characterize the degree of mixing at different axial locations in the gasper-induced jet, the CFD model was also used to explore mixing layer thickness development in the flow. As recommended by Pope (2000), the present study defined the mixing layer thickness as $\lambda = x_{0.1} - x_{0.9}$, where $x_{0.1}$ and $x_{0.9}$ are the radial locations at which the z-velocities are 0.1 and 0.9, respectively, of the maximum velocity at a particular z location. As shown in Figure 10, the normalized mixing layer thickness λ/D was plotted against z/D for cases 1 through 5 (for which the details are listed in Table 2), in order to determine the influence of gasper inlet velocity and opening size. Good self-similarity can be seen in the mixing layer thickness for different inlet velocities (U_0) and opening sizes (δ). The mixing layer thickness increased continuously along the jet axis, which can be explained by the spread of coherent structures in the flow (Pope 2000): when the gasper-induced jet was discharged into the quiescent surroundings, disturbances triggered and amplified the vortical structures, which merged into coherent structures; these coherent structures grew in size as they were transported downstream, which greatly enhanced the mixing process. The growth in the mixing layer thickness, however, was divided into three zones as the slope changed: zones 1 and 3 had the same slope, while zone 2 had a slightly lesser slope. The difference among zones can be explained by the transition from the developing region to the fully developed region in the jet flow.

Table 2. Parameters of the cases used to investigate the influence of inlet velocity and opening size on gasper-induced jet flow.

Case #	Inlet velocity (U_0, m/s)	Reynolds # (Re)	Opening size (δ, mm)

1(Original)	40	32,102	0.9
2	60	48,153	0.9
3	80	64,204	0.9
4	40	32,102	0.7
5	40	32,102	1.1

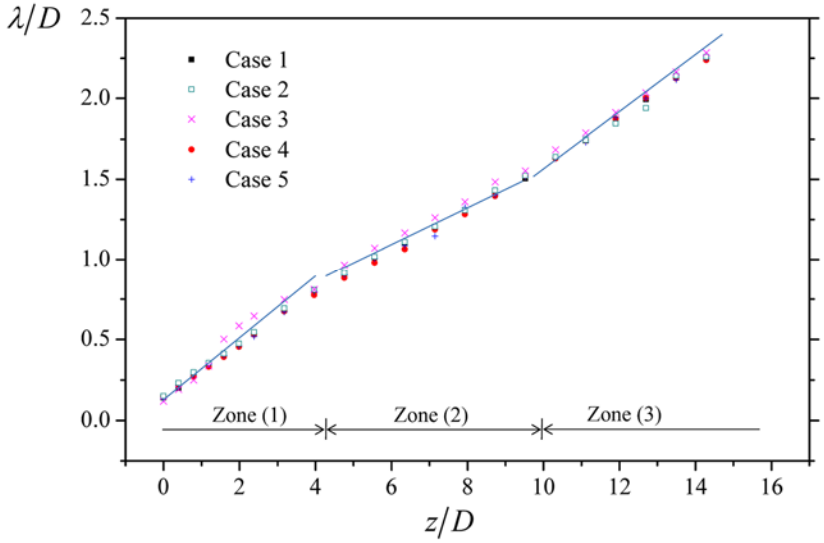

Fig. 10 Mixing layer thickness at locations in the downstream region of the jet

3.3 Mathematical modeling of the gasper-induced jet

3.3.1 Development of empirical equations

i. Centerline velocity

As discussed in Section 3.2, various cases were designed using the validated CFD model to explore the influence of inlet velocity and opening size on mixing layer thickness. The same set of cases was used to investigate the impact of inlet velocity and opening size on centerline velocity distribution.

Figure 11 (a) compares the centerline velocity profiles of the gasper-induced jet flow with three different inlet velocities. The general trends of the profiles are very similar. The results also show that, with the same gasper geometry, the peak locations under various initial velocities are very close to each other, which agrees with the experiments in Dai et al. (2015). Furthermore, a plot of normalized centerline velocity $U_c/U_{\max}$ versus normalized axial location $(z-z_{peak})/D$ (Figure 11(b)) shows that these velocity profiles are closely matched with one another, especially as the velocity decayed along the centerline. This indicates that the flow characteristics after the

peak location, where jet flow was more developed, tended to follow a more uniform pattern than in the region where flow was still developing.

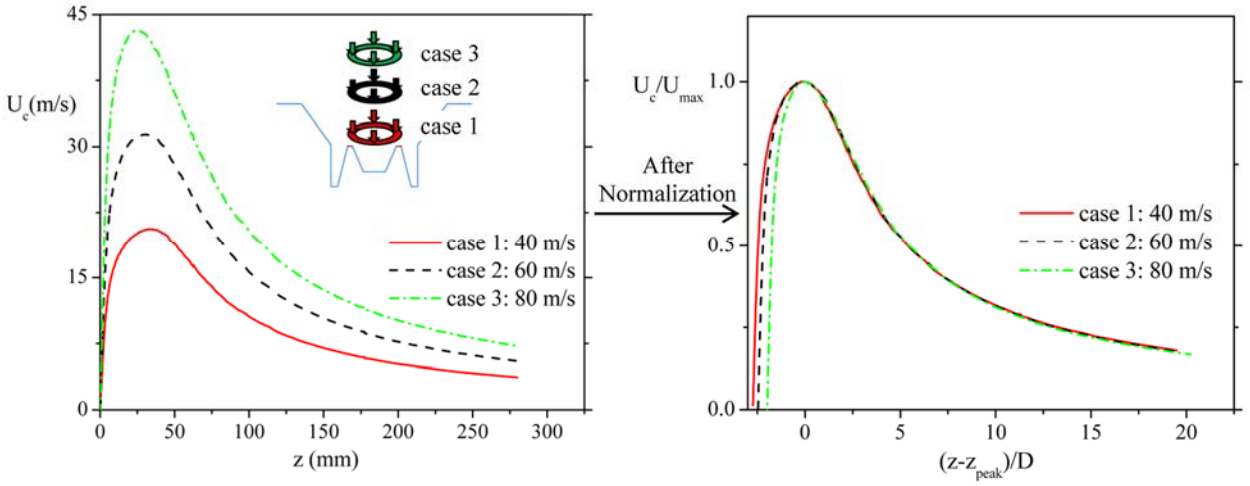

(a) (b)

Fig. 11 Centerline velocity profiles with different inlet velocities: (a) before normalization and (b) after normalization.

Figure 12 compares the centerline velocity distributions and normalized profiles in Cases 1, 4, and 5, where the gasper was adjusted to different opening sizes. As with the uniform pattern in Figure 11(b), the normalized velocity profiles, $U_c/U_{\max}$ versus $\left(z-z_{peak}\right)/D$, also collapsed into a single curve. The z_{peak} values, however, were found to increase as the opening size increased according to Figure 12(a). This trend agrees with the results illustrated in Dai et al. (2015), and the reason might be that under the same initial velocity, a larger opening size led to greater fluid momentum from the gasper inlet, which pushed the merging point forward. Meanwhile, due to greater momentum at larger opening, maximum axial velocity was also found to be larger as opening increased.

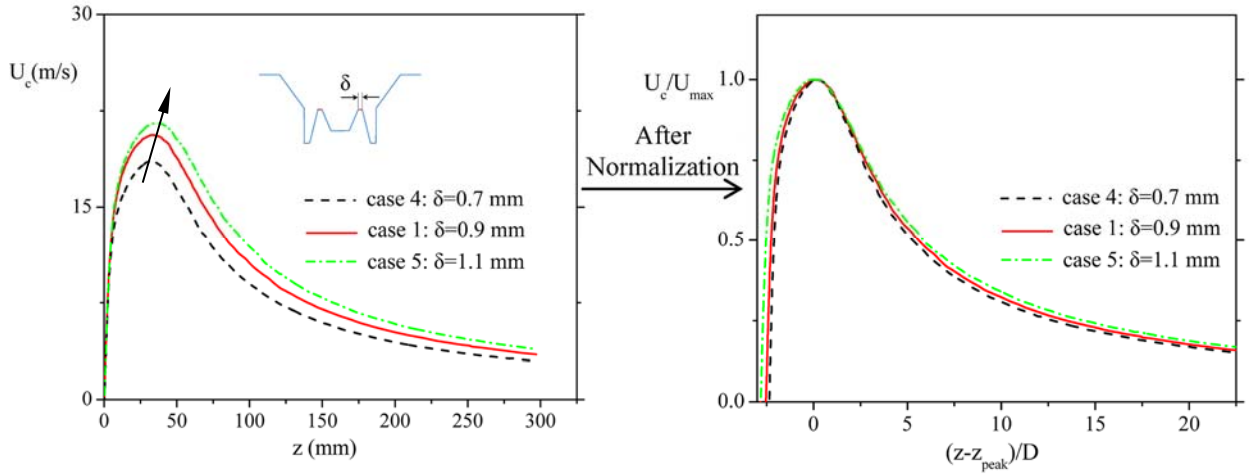

(a) (b)

Fig. 12 Centerline velocity profiles with different opening sizes: (a) before normalization and (b) after normalization.

The analysis above indicates that the normalized centerline velocity profile is independent of the inlet velocity and inlet opening. Thus, this study developed an empirical equation for the centerline velocity. As mentioned in Section 2.4, the flow developments before and after the merging point are completely different, and thus the centerline velocity before and after the peak velocity location can be modeled separately as a piecewise function. Before the peak velocity location, a cubic function was used to describe the velocity profile, which increases dramatically at first, and then gradually becomes slower as the location becomes closer to the peak location. Experimental data (Dai et al. 2015) was used for curve fitting, which yielded the normalized velocity profile $\frac{U_c}{U_{\max}} = g(\bar{z}) = 1.49\bar{z}^3 + 2.31\bar{z}^2 + 1.19\bar{z} + 1.18$, where $\bar{z} = \left(z - z_{peak}\right)/D$. The centerline velocity starts to decay after the flow has reached its peak centerline velocity. Previous studies (Hussein et al. 1994; Panchapakesan 1993) described the relationship between normalized centerline velocity and normalized centerline location in a round isothermal jet using a rational function whose denominator was one degree higher than the numerator. Similarly, the present study has proposed a rational function to describe the velocity profile when $\bar{z} > 0$. Fitting the proposed rational function with experimental data yields $g(\bar{z}) = \frac{0.42\bar{z} + 1}{0.12\bar{z}^2 + 0.37\bar{z} + 1}$ when $\bar{z} > 0$.

In summary, the new gasper centerline velocity formula (GCVF) is

$$\frac{U_c}{U_{\max}} = g(\bar{z}) = \begin{cases} 1.49\bar{z}^3 + 2.31\bar{z}^2 + 1.19\bar{z} + 1.18, & \bar{z} < 0 \\ \dfrac{0.42\bar{z} + 1}{0.12\bar{z}^2 + 0.37\bar{z} + 1}, & \bar{z} > 0 \end{cases}. \qquad (2)$$

Figure 13 compares the centerline velocity predicted by the empirical equation, the simulation results, and the experimental data. It can be seen that the proposed empirical equation is able to predict the centerline velocity profile with good accuracy.

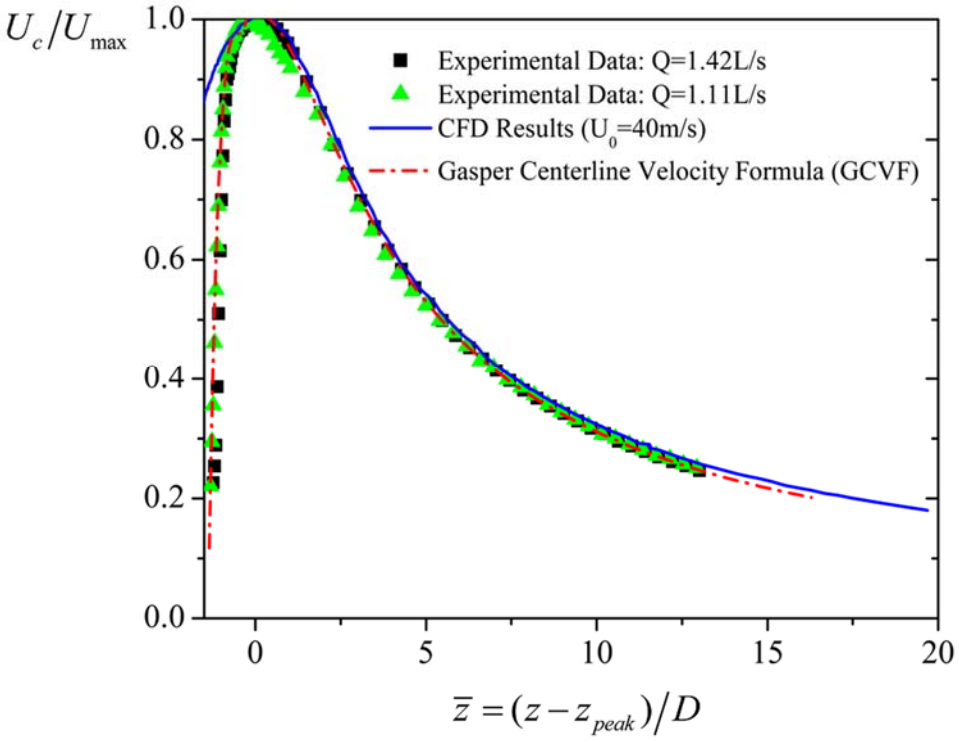

Fig. 13 Comparison of the centerline velocity profiles obtained from the empirical equation, simulation results, and experimental data from Dai et al. (2015).

ii. Radial velocity profile

After the merging point, the radial velocity profiles from the CFD calculations exhibited self-similarity characteristics, as shown in Figure 14. This study further developed an empirical equation for calculating the radial velocity after the merging point. Papanicolaou and List (1984), and Corrsin and Uberoi (1951) reported a Gaussian velocity profile at a downstream location in a turbulent round jet. Assuming that the lateral velocity profile after the merging point follows the same pattern, the present study used a Gaussian equation to describe the relationship between the normalized z velocity and normalized lateral location. Experimental data was utilized to determine the parameters in the Gaussian equation. This yielded the gasper downstream radial velocity profile (GDRP):

$$\frac{U_z}{U_c} = e^{-\frac{5}{8}\chi^2}, \tag{3}$$

where normalized x location $\chi = x/x_{1/2}$, and U_z is the z-direction mean velocity at a given point.

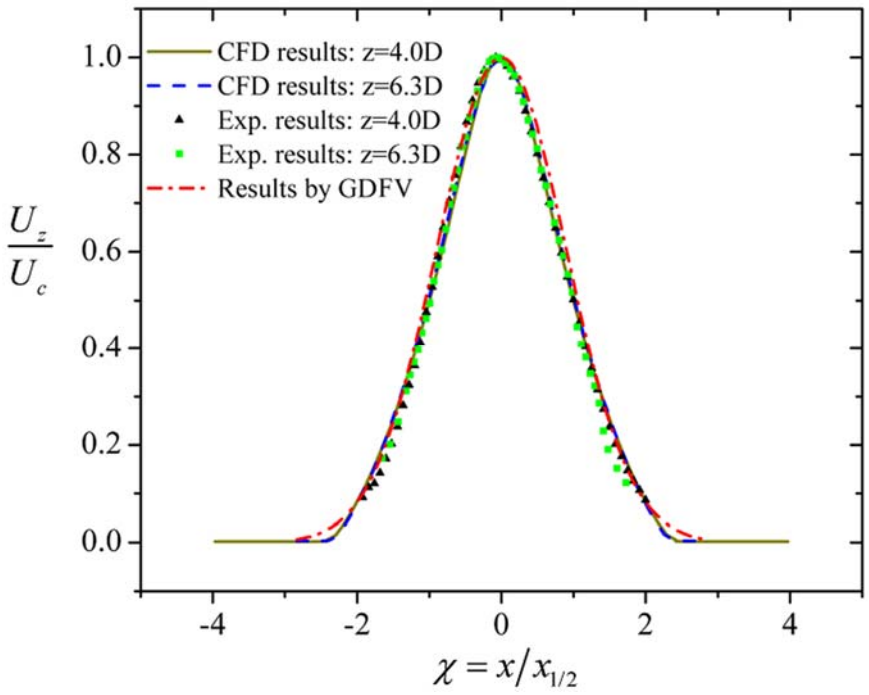

Fig. 14 Comparison of GDRP result, experimental data, and CFD result

As shown in Figure 14, the normalized lateral velocity profiles calculated by the empirical equation were in good agreement with the CFD calculation and the experimental data.

For application of Eq. (3), $x_{1/2}$ needed to be pre-determined. Kwon and Seo (2005) reported a linear relationship between $x_{1/2}$ and the axial location z in a free round jet. Figure 15 is a plot of the normalized jet half width $x_{1/2}/D$ versus $\overline{z}$ from CFD results for the current gasper-induced jet flow. In the downstream region, a strong linear relationship can be observed between $x_{1/2}/D$ and $\overline{z}$, which is similar to that in a round jet. However, in the vicinity of the gasper inlet, the linear relationship does not exist. This investigation used a quadratic equation to describe the development of $x_{1/2}/D$ near the inlet region.

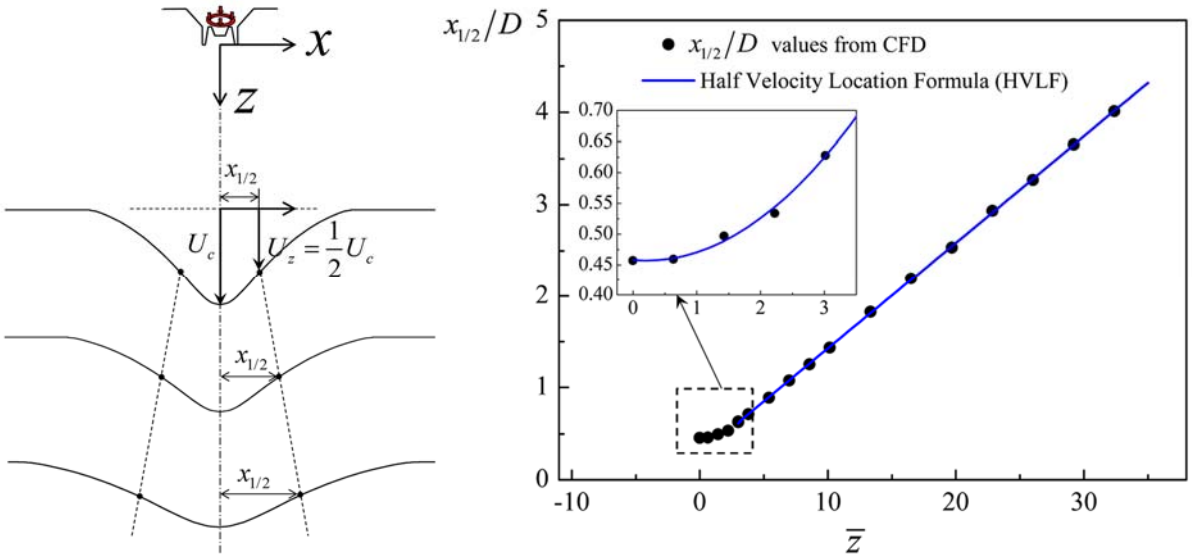

(a) (b)

Fig. 15 (a) Sketch of lateral velocity profile and (b) relationship between $x_{1/2}/D$ and $\overline{z}$.

From these observations, this study developed an empirical equation to describe $x_{1/2}$:

$$\frac{x_{1/2}}{D} = h(\overline{z}) = \begin{cases} 0.021\overline{z}^2 - 0.0087\overline{z} + 0.478, & \overline{z} \le 3 \\ 0.116\overline{z} + 0.270, & \overline{z} > 3 \end{cases}. \quad (4)$$

The empirical formulas (Eqs. 2 through 4), when utilized together, can provide useful information about velocity in the gasper-induced flow field, and thus can be helpful for the analysis of gasper-induced jets and the design of gaspers.

iii. $U_{\max}$ and z_{peak}

Empirical equations (2) and (4) are dependent on two key parameters, the peak centerline velocity $U_{\max}$ and its location z_{peak}, which change from case to case. In order to make the mathematical models complete, this study further explored the relationships between these parameters and two gasper boundary conditions that can be easily measured: initial air flow rate $\dot{Q}_0$ and opening area A.

Section 3.2 demonstrated that the peak in the centerline velocity profile was due to rapid entrainment of ambient fluid after z-stagnation point z_{s2}. Moreover, Ricou and Spalding (1961)

have shown that in a round jet, the entrainment amount is proportional to $\sqrt{M_0}$, where M_0 is the initial momentum flux at the jet nozzle. Thus, this research has assumed that $U_{\max}$ is correlated with $\sqrt{M_0}$. With the use of dimensional analysis, the relationship can be expressed as

$$\rho D^2 U_{\max}^2 = K_1 M_0 \tag{5}$$

where ρ is air density and K_1 is a dimensionless value.

Since $M_0 = \rho U_0^2 A$ and $\dot{Q}_0 = U_0 A$, the above equation can be further expressed as

$$U_{\max} = \sqrt{K_1}\sqrt{\frac{\dot{Q}_0^2}{AD^2}} \tag{6}$$

Figure 16a is a plot of $U_{\max}$ versus $\frac{\dot{Q}_0^2}{AD^2}$, at opening sizes of 0.7 mm, 0.9 mm, 1.1 mm, and 1.3 mm. For each opening size, five U_0 values were tested: 40 m/s, 50 m/s, 60 m/s, 70 m/s and 80 m/s. These 20 sample points were well fitted to the power equation with $R^2 = 0.95$:

$$U_{\max} = 0.93\sqrt{\frac{\dot{Q}_0^2}{AD^2}} \tag{7}$$

or

$$\frac{U_{\max}}{\dot{Q}_0/A} = 0.93\sqrt{\frac{A}{D^2}} \tag{8}$$

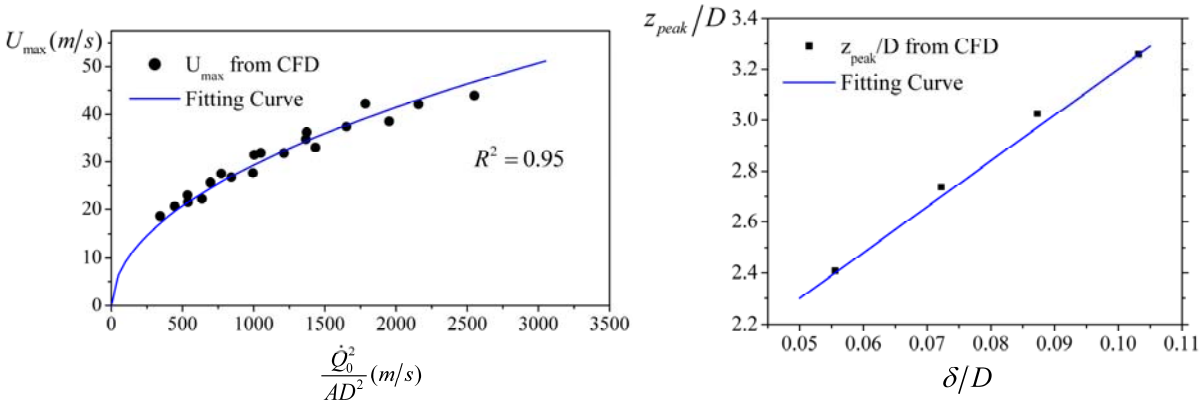

(a) (b)

Fig. 16 The relationship between (a) $U_{\max}$; (b) z_{peak} and gasper initial conditions

On the other hand, according to Figures 11 and 12, z_{peak} was correlated with gasper opening size but not initial velocity. In Figure 16b, z_{peak} is plotted against δ at four gasper opening sizes. The results show that z_{peak} increased almost linearly with δ. The correlation between peak velocity location and opening size can be fitted by a straight line:

$$\frac{z_{peak}}{D} = 18.0\frac{\delta}{D} + 1.4 \tag{9}$$

which yields

$$\frac{z_{peak}}{D} = 18.0\frac{A}{\pi D^2} + 1.4 \tag{10}$$

Formulas (8) and (10) supplement Equations (2) through (4) and thus bring to completion the development of empirical equations for gasper-induced jet velocity.

3.3.2 Virtual Origin Model

Previous investigations have reported that because of self-preserving properties in the developed flow region, U_0/U_c is proportional to $(z - z_0)/D$ in the downstream regions of a round jet (Hussein et al. 1994; George et al. 1989) and an annular jet (Chigier and Beer 1964), where z_0 is defined as the virtual origin. In particular, z_0 represents the z-intercept of the straight line, U_0/U_c versus z/D, and it represents a point source of momentum of the jet. In analogy, the present study has also explored the relationship between the inverse of centerline velocity and axial distance in a gasper-induced jet for cases demonstrated in Table 2, by plotting U_0/U_c against z/D as shown in Figure 17. The results indicate a strong linear relationship between U_0/U_c and z/D after $z = 7D$, and the straight lines share a common z-intercept: $0.2D$. The relationship is independent of initial velocity, but the slope of the straight line decreases as gasper opening size increases.

Figure 17 also shows the relationship between slope and opening size, and a fitting linear equation can be used to describe the relationship (an additional case with $\delta = 1.3mm$ was included for the linear fitting). On the basis of the above relationships, the virtual origin model for gasper-induced jet flow can be defined as:

$$\frac{U_0}{U_c} = (0.74 - 3.53\frac{\delta}{D})\frac{z-0.2D}{D}$$

$$= (0.74 - 3.53\frac{A}{\pi D^2})\frac{z-0.2D}{D} \qquad (11)$$

This simple model is able to predict centerline velocity with good accuracy in the downstream region of a gasper-induced jet. The axial velocities as a function of radial distance can be determined from Eq. (3) after the centerline velocity has been identified.

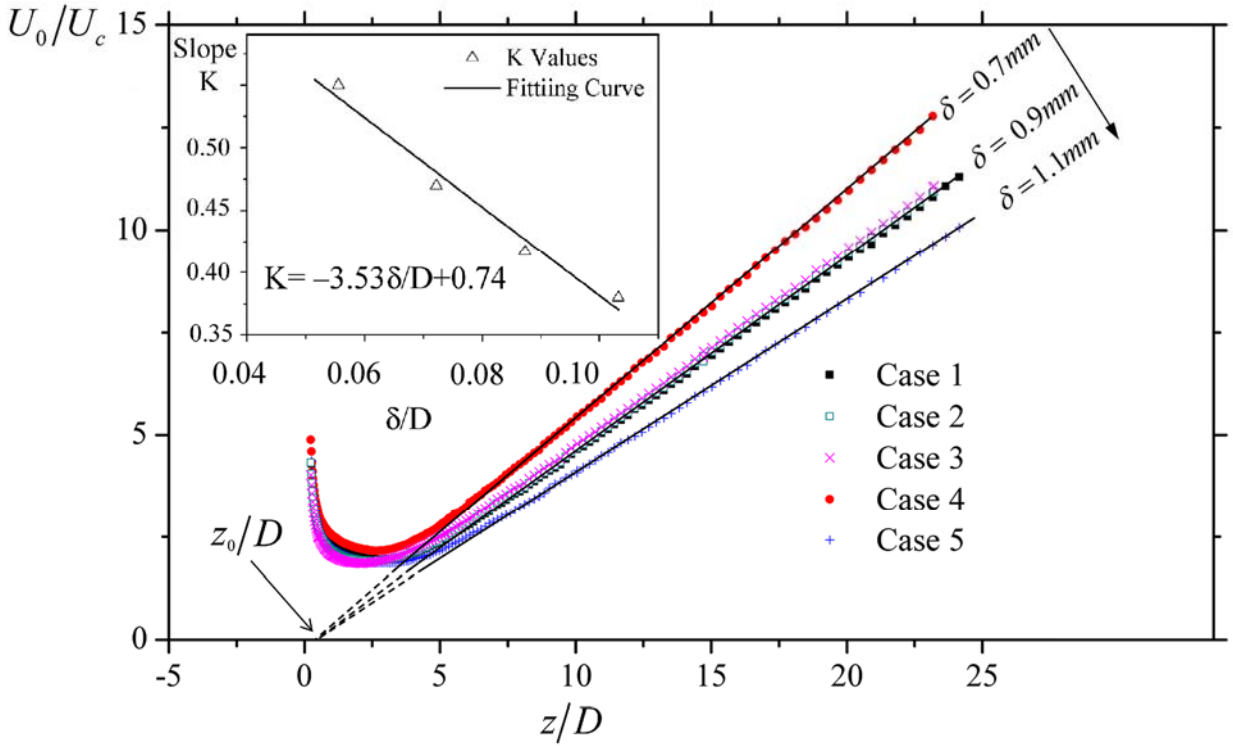

Fig. 17 Relationship between U_0/U_c and z/D in a gasper-induced jet (Inset: Slope K versus opening size)

In comparison with the empirical equations method described in Section 3.3.1, the virtual origin model is a much simpler method that is able to predict the airflow velocity in the developed region of a gasper-induced jet. This model was created with the assumption that the jet originates from a point source of momentum spread linearly in the developed region, and it has also been used to predict the entrainment ratio, as discussed in the following section.

3.4 Entrainment analysis and impact of gasper-induced jet flow on cabin air quality

An important flow phenomenon in a gasper-induced jet is entrainment. In a previous study (Ricou and Spalding 1960), the entrainment ratio was calculated as $\varepsilon = \frac{\dot{m}}{\dot{m}_0}$, where $\dot{m}_0$ is the mass flow rate at the jet nozzle, and $\dot{m}$ is the mass flow rate at a certain point downstream from the jet's main stream. In the current study, the fresh air ratio is defined as $\eta = \frac{1}{\varepsilon} = \frac{\dot{m}_0}{\dot{m}}$, in order to quantify the percentage of fresh air (the air that is discharged from the gasper nozzle) at a location in the downstream region of the jet. The fresh air ratio can be predicted by use of the validated CFD model, the empirical equations, and the developed virtual origin model, as follows.

(1) CFD method

With the validated CFD model, $\dot{m}$ can be simply evaluated by reporting the flow rate at different downstream locations inside the envelope formed by z-stagnation lines, which were defined in Section 3.4. The fresh air ratio η can then be calculated by dividing the gasper inlet mass flow rate $\dot{m}_0$ by $\dot{m}$ at each downstream location.

(2) Empirical equations

On the basis of the empirical equations for the centerline and radial velocity profiles, the current study calculated the airflow rate at a certain cross-section as follows.

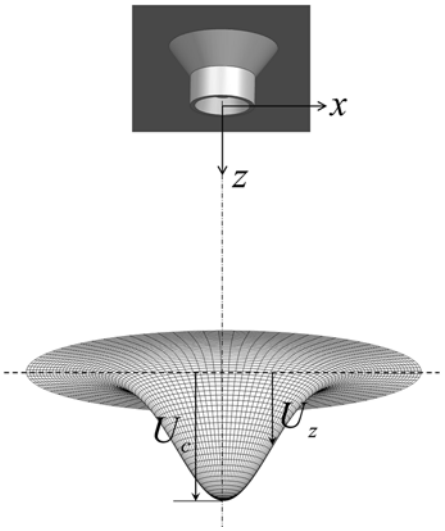

Fig. 18 Z-direction velocity profile at a location in the downstream region of the gasper-induced jet flow

Figure 18 demonstrates a 3D schematic of the Gaussian shape profile of U_z at a downstream location. The air flow rate at a cross section can be calculated by integrating U_z over the whole area of the cross section. When the GCVF and GDRP formulas are combined, the integration can be performed as follows:

$$\begin{aligned}\dot{Q} &= \iint U_z dA = \int_0^\infty U_z \cdot 2\pi x dx = \int_0^\infty \exp\left(-\frac{5}{8}\chi^2\right) U_c \cdot 2\pi x dx \\ &= \int_0^\infty \exp\left(-\frac{5}{8}\left(\frac{x}{x_{1/2}}\right)^2\right) U_c \cdot 2\pi x dx \\ &= \int_0^\infty \exp\left(-\frac{5}{8}\left(\frac{x}{h(\overline{z})D}\right)^2\right) g(\overline{z}) U_{\max} \cdot 2\pi x dx\end{aligned} \tag{12}$$

Thus, the fresh air ratio can be calculated as:

$$\begin{aligned}\eta &= \frac{\dot{Q}(z=0)}{\dot{Q}(z)} = \frac{\dot{Q}(z=0)}{\dot{Q}(\overline{z}=0)} \cdot \frac{\dot{Q}(\overline{z}=0)}{\dot{Q}(z)} \\ &= \frac{\dot{Q}(z=0)}{\dot{Q}(\overline{z}=0)} \cdot \frac{\int_0^\infty \exp\left(-\frac{5}{8}\left(\frac{x}{h(0)D}\right)^2\right) g(0) U_{\max} \cdot 2\pi x dx}{\int_0^\infty \exp\left(-\frac{5}{8}\left(\frac{x}{h(\overline{z})D}\right)^2\right) g(\overline{z}) U_{\max} \cdot 2\pi x dx}\end{aligned} \tag{13}$$

Although it is not possible to express the integral analytically, the definite integral can still be calculated using Newton-Cotes formulae (Abramowitz and Ategun 1972).

(3) Virtual origin model

George (1989) illustrated that in a fully developed jet, the entrainment ratio $\varepsilon = \frac{\dot{m}}{\dot{m}_0}$ had a linear relationship with jet axial distance, and the straight line intersected with the abscissa at the virtual origin. Moreover, Ricou and Spalding (1961) used experimental results to conclude that the slope of the straight line was $0.32(\frac{\rho_1}{\rho_0})^{\frac{1}{2}}$, where ρ_1 was fresh fluid density and ρ_0 was the density of ambient fluid. Given that the current gasper-induced flow is homogenous, and by use of the virtual origin model developed in Section 3.3.2, this relationship can be expressed as

$$\varepsilon = \frac{\dot{m}}{\dot{m}_0} = 0.32\frac{z - 0.2D_e}{D_e} \tag{14}$$

where the equivalent diameter D_e is defined so that the mass flow rate discharged through the current gasper nozzle is equal to the mass flow rate discharged from a round nozzle with diameter D_e. When the continuity equation for mass is employed,

$$\dot{m}_0 = \pi D\delta U_0 = \pi(\frac{D_e}{2})^2 U_0 \tag{15}$$

This expression leads to $D_e = \sqrt{4\delta D}$. Thus, the fresh air ratio can be calculated by use of the virtual origin model as:

$$\eta = \frac{1}{\varepsilon} = \frac{1}{0.32(z/\sqrt{4\delta D} - 0.2)}. \tag{16}$$

Figure 19 shows the fresh air ratio as predicted by the CFD model, empirical equations, and virtual origin model. Since the flow velocity predicted by CFD has been validated in both the developing and developed regions, the fresh air ratio calculated from air flow rates at different cross sections is considered to be accurate. Overall, the fresh air ratio dropped quickly after air was discharged from gasper nozzle. Both the empirical equation method and virtual origin model predicted the fresh air ratio results with good accuracy, although the results of the empirical equations matched slightly better with the CFD results.

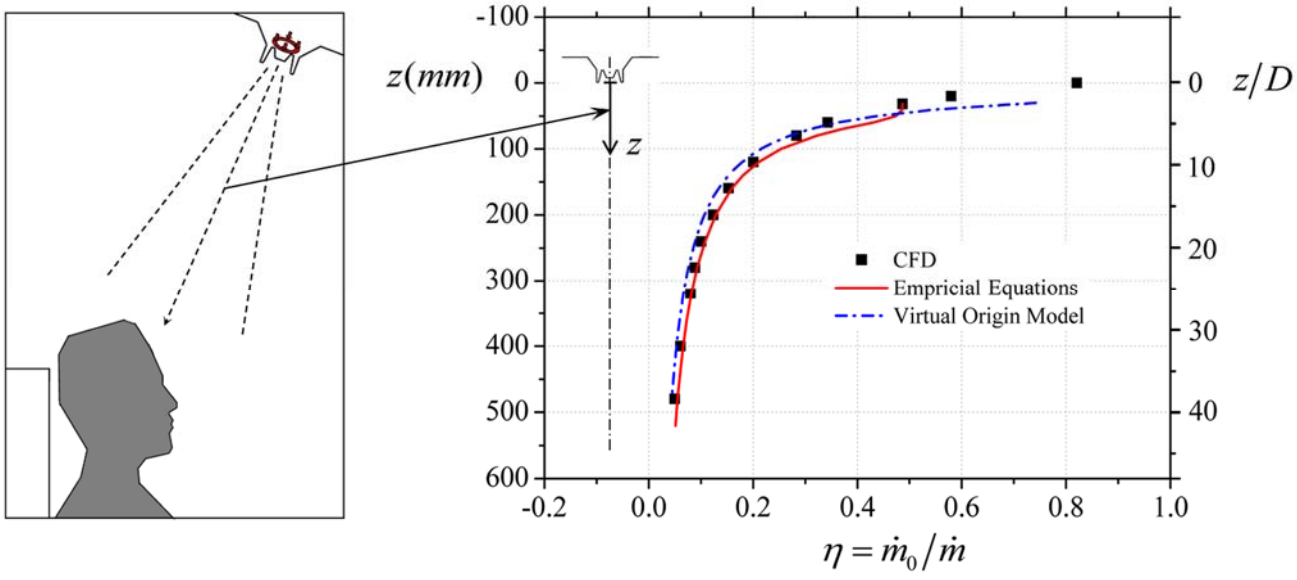

Fig. 19 Relationship between the gasper-induced airflow ratio and the distance from the inlet.

The distance between a gasper and the passenger's breathing zone may vary greatly. This study used the value of 0.48 m as recommended by Anderson (2012). The results from all three methods (Fig. 19) show that the gasper-induced airflow ratio was about 5% in the breathing zone of the passenger. This means that, when the gasper was turned on, about 5% of the air in the breathing zone was from the gasper, while 95% of the air was from the cabin. This result indicates that the jet flow induced by a gasper has a very minor influence on the air quality in a passenger's breathing zone.

5 Discussion

5.1 Comparison of the three modeling methods

In the present study, three modeling methods (CFD, empirical equations, and the virtual origin model) were used to investigate the flow characteristics of a gasper-induced jet. The predicting ability and prediction time of the three methods are summarized and evaluated in Table 3, where stars have been used to rate prediction accuracy and solution time. Overall, the CFD method yielded the most accurate results, and it was able to predict additional flow features such as pressure and turbulence intensity. However, this method required a significant amount of time for setup and numerical computation. The empirical equations also provided good predictions of velocity, as well as predicting the entrainment ratio in the developed region, although this method was not able to predict other flow features. The virtual origin model was the simplest and thus the least time-consuming method, and it was capable of predicting velocity and entrainment ratio in most parts of the gasper-induced jet region. Generally speaking, the CFD method is recommended when other flow features are needed in addition to velocity, whereas the virtual origin model is recommended when only velocity or entrainment information in the downstream region of a gasper-induced jet is required.

Table 3 Comparison of three modeling methods in terms of prediction ability and time

Method	Velocity prediction accuracy			Entrainment ratio prediction accuracy		Ability to predict pressure or turbulence features	Time needed to obtain solution
	Developing region (centerline)	Developed region (centerline)	Downstream radial distribution	Developing region	Developed region		
CFD	☆☆☆☆	☆☆☆☆☆	☆☆☆☆☆	☆☆☆☆	☆☆☆☆☆	Yes	☆☆☆☆☆
Empirical equations	☆☆☆☆	☆☆☆☆☆	☆☆☆☆☆	Not capable	☆☆☆☆	No	☆☆
Virtual	Not capable	☆☆☆☆☆	☆☆☆☆	Not	☆☆☆	No	☆

origin model			☆	capable	☆		

5.2 Limitations

This study modeled a gasper-induced free jet. Although such a jet usually has a much higher velocity than the ambient airflow, it is still possible that in a real case the jet flow features would be influenced by other flows, such as the flow from the main diffuser in an aircraft cabin or the breathing of passengers. In this study, it was assumed that ambient flow had only a minor impact on the jet.

In addition, this study assumed that the gasper-induced jet was an isothermal flow. In reality, however, ambient air, passengers' heads, and the aircraft cabin walls may have different temperatures than that of the jet. When making conclusions about the impact of gasper-induced jet flow on the air quality in the breathing zone, this investigation assumed that temperature variations did not have a great influence on the flow in the jet mainstream.

6 Conclusions

This study has led to the following conclusions:

(1) The CFD model with the SST $k-\omega$ model can provide good predictions of gasper-induced jet flows. The velocity profiles in the transverse direction began as "double-peak" curves and were transformed to a "single-peak" curve after the merging point. The velocity profiles in the developing region were very different from those for free round jet flow.

(2) At the onset of a gasper-induced jet, the pressure gradient maintained reverse flow and generated vortices. Subsequently, the pressure dropped dramatically, which caused the centerline velocity to continuously increase until it reached the peak value. The mixing layer thickness continued to increase in the direction of the gasper-induced jet.

(3) The empirical equations and virtual origin model developed in this study were able to predict gasper-induced jet velocities with good accuracy, and they were much less time consuming than the prediction with the CFD method. In comparison with the empirical equations, the virtual origin model was simpler in expression, whereas the empirical equations provided better centerline velocity prediction in the developing region. However, the CFD method was able to provide more comprehensive flow characteristics such as pressure and turbulence intensity in the flow field, which neither the empirical equations nor the virtual origin model were able to predict.

(4) Entrainment ratios predicted by the three modeling methods in the developed region agreed well with one another. The results showed that when the gasper was turned on, more than 90% of the air in the passenger's breathing zone was entrained from the surroundings. Thus, a gasper-induced jet has only a very minor impact on the air quality in a passenger's breathing zone.

Acknowledgement

The research presented in this paper was partially supported by the National Basic Research Program of China (the 973 Program) through Grant No. 2012CB720100.

References

Abramowitz, M. and I. A. Stegun (Eds.). 1964. *Handbook of Mathematical Functions: With Formulas, Graphs, and Mathematical Tables.* No. 55. Mineola, NY: Courier Corporation.

Anderson, M. D. 2012. "Effect of gaspers on airflow patterns and the transmission of airborne contaminants within an aircraft cabin environment." *Dissertation,* Kansas State University.

ANSYS Inc. 2011. ANSYS Fluent Theory Guide, Release 14.0 [online]. Available from http://www.ansys.com [Accessed 8 October 2013]

Baker, A. J., S. C. Ericson, J. A. Orzechowski, K. L. Wong, and R. P. Garner. 2006. "Validation for CFD prediction of mass transport in an aircraft passenger cabin." *Federal Aviation Administration Oklahoma City OK Civil Aeromedical Inst.*

Baker, M. G., C. N. Thornley, C. Mills, S. Roberts, S. Perera, J. Peters, A. Kelso, I. Barr, and N. Wilson. 2010. "Transmission of pandemic A/H1N1 2009 influenza on passenger aircraft: Retrospective cohort study." *BMJ* 340.

Chigier, N.A. and J. M. Beer. 1964. "The flow region near the nozzle in double concentric jets." *Journal of Fluids Engineering* 86(4): 797-804.

Corrsin, S., and M. S. Uberoi. 1951. Spectra and diffusion in a round turbulent jet. *Journal of Propulsion and Power* 16 (4): 676-686.

Dai, S., H. Sun, W. Liu, Y. Guo, N. Jiang, and J. Liu. 2015. "Experimental study on characteristics of the jet flow from an aircraft gasper." *Building and Environment* 93: 278-284.

Fan, Q., L. Wang, and F. Wang. 2005. "3D simulation of the plasma jet in thermal plasma spraying." *Journal of Materials Processing Technology* 166 (2): 224-229.

Gao, N. P., and J. L. Niu. 2008. "Personalized ventilation for commercial aircraft cabins." *Journal of Aircraft* 45(2): 508-512.

García-Villalba, M., J. Fröhlich, and W. Rodi. 2006. "Identification and analysis of coherent structures in the near field of a turbulent unconfined annular swirling jet using large eddy simulation." *Physics of Fluids (1994-present)* 18(5): 055103.

George, W. K., P. D. Beuther, and A. Shabbir. 1989. "Polynomial calibrations for hot wires in thermally varying flows." *Experimental Thermal and Fluid Science* 2(2): 230-235.

Guo, Y., N. Jiang, S. Yao, S. Dai, and J. Liu. 2014. "Turbulence measurements of a personal airflow outlet jet in aircraft cabin." *Building and Environment* (82): 608-617.

Gupta, J. K., C.-H. Lin, and Q. Chen. 2011. "Can gaspers provide protection from airborne contaminants to the occupants in an airliner cabin?" *Proceedings of the 12th International Conference on Indoor Air Quality and Climate (Indoor Air 2011)*, Austin, Texas.

Hinze, J. O. 1975. *Turbulence*. New York: McGraw-Hill.

Hussein, H. J., S. P. Capp, and W. K. George. 1994. "Velocity measurements in a high-Reynolds-number, momentum-conserving, axisymmetric, turbulent jet." *Journal of Fluid Mechanics* 258: 31-75.

International Air Transport Association (IATA). 2013. "Airlines Expect 31% Rise in Passenger Demand by 2017" [online]. Available from http://www.iata.org/pressroom/pr/pages/2013-12-10-01.aspx [Accessed January 2015]

International Civil Aviation Organization (ICAO). 2012. "Annual Passenger Total Approaches 3 Billion According to ICAO 2012 Air Transport Results" [Online]. Available from http://www.icao.int/ Newsroom /Pages/annual-passenger-total-approaches-3-billion-according-to-ICAO-2012-air-transport-results.aspx [Accessed January 2015]

Kwon, S. J., and I. W. Seo. 2005. "Reynolds number effects on the behavior of a non-buoyant round jet." *Experiments in Fluids* 38(6): 801-812.

Li, Y., G. M. Leung, J. W. Tang, X. Yang, C. Chao, J. H. Lin, J. W. Lu, P. V. Nielsen, J. L. Niu, H. Qian, A. C. Sleigh, H. J. Su, J. Sundell, T. W. Wong, and P. L. Yuen. 2007. "Role of ventilation in airborne transmission of infectious agents in the built environment – A multidisciplinary systematic review." *Indoor Air* 17 (1): 2–18.

Melikov, A., T. Ivanova, and G. Stefanova. 2012. "Seat headrest-incorporated personalized ventilation: Thermal comfort and inhaled air quality." *Building and Environment* 47: 100-108.

Menter, F. R. 1994. "Two-equation eddy-viscosity turbulence models for engineering applications. " *AIAA Journal* 32(8): 1598-1605.

Moore, E. M., R. L. Shambaugh, and D. V. Papavassiliou. 2004. "Analysis of isothermal annular jets: Comparison of computational fluid dynamics and experimental data." *Journal of Applied Polymer Science* 94(3): 909-922.

Olsen, S. J., H. L. Chang, T. Y. Y. Cheung, A. F. Y. Tang, T. L. Fisk, S. P. L. Ooi, H. W. Kuo, D. D. S. Jiang, K. T. Chen, J. Lando, K. H. Hsu, T. J. Chen, and S. F. Dowell. 2003. "Transmission of the severe acute respiratory syndrome on aircraft." *New England Journal of Medicine* 349(25): 2416-2422.

Olsson, M., and L. Fuchs. 1996. "Large eddy simulation of the proximal region of a spatially developing circular jet." *Physics of Fluids (1994-present)* 8(8): 2125-2137.

Panchapakesan, N. R., and J. L. Lumley. 1993. "Turbulence measurements in axisymmetric jets of air and helium. Part 1. Air jet." *Journal of Fluid Mechanics* 246: 197-223.

Papanicolaou, P. N., and E. J. List. 1988. "Investigations of round vertical turbulent buoyant jets." *Journal of Fluid Mechanics* 195: 341-391.

Patankar, S. 1980. *Numerical Heat Transfer and Fluid Flow*. Boca Raton, FL: CRC Press.

Pope, S. B. 2000. *Turbulent Flows*. Cambridge: Cambridge University Press.

Ricou, F. P., and D. B. Spalding. 1961. "Measurements of entrainment by axisymmetrical turbulent jets." *Journal of Fluid Mechanics* 11(01): 21-32.

Rehab, H., E. Villermaux, and E. J. Hopfinger. 1997. "Flow regimes of large-velocity-ratio coaxial jets." *Journal of Fluid Mechanics* 345: 357-381.

Shi, Z., J. Chen, and Q. Chen. 2015. "On the turbulence models and turbulent Schmidt number in simulating stratified flows. " *Journal of Building Performance Simulation*: 1-15.

Touloukian, Y. S., S. C. Saxena, and P. Hestermans. 1975. "Thermophysical Properties of Matter-the TPRC Data Series. Volume 11. Viscosity." *Thermophysical and Electronic Properties Information Analysis Center Lafayette IN.*

Wang, A., Y. Zhang, Y. Sun, and X. Wang. 2008. "Experimental study of ventilation effectiveness and air velocity distribution in an aircraft cabin mockup." *Building and Environment* 43(3): 337-343.

Warda, H. A., S. Z. Kassab, K. A. Elshorbagy and E. A. Elsaadawy. 1999. "An experimental investigation of the near-field region of free turbulent round central and annular jets*." Flow Measurement and Instrumentation* 10 (1): 1-14.

Wilcox, D. C. 1998. *Turbulence modeling for CFD*. Vol. 2. La Canada, CA: DCW industries.

White, F. M., and I. Corfield. 1991. *Viscous Fluid Flow*. Vol. 3. New York: MacGraw-Hill.

Wille, R., and H. Fernholz. 1995. "Report on the first European Mechanics Colloquium, on the Coanda effect." *Journal of Fluid Mechanics* 23(04): 801-819.

Wu, C., and N. A. Ahmed. 2011. "Numerical study of transient aircraft cabin flowfield with unsteady air supply. " *Journal of Aircraft* 48(6): 1994-2001.

You, R., J. Chen, Z. Shi, W. Liu, C. H. Lin, D. Wei, and Q. Chen. 2016. "Experimental and numerical study of airflow distribution in an aircraft cabin mock-up with a gasper on." *Journal of Building Performance Simulation*: 1-12.

Zhang, T., and Q. Chen. 2007. "Novel air distribution systems for commercial aircraft cabins," *Building and Environment*, 42(4), 1675-1684.

Zítek, P., T. Vyhlídal, G. Simeunović, L. Novakova, and J. Čížek. 2010. "Novel personalized and humidified air supply for airliner passengers." *Building and Environment* 45(11): 2345-2353.